Journal of Materials Science: Materials in Electronics (2020) 31:5198–5204
https://doi.org/10.1007/s10854-020-03079-2

Current-transport mechanisms in the Au/GaSe:Nd Schottky contact

Hüseyin Ertap[1] · Hatice Kacus[2] · Sakir Aydogan[2,3] · Mevlut Karabulut[4]

Received: 21 November 2019 / Accepted: 10 February 2020 / Published online: 19 February 2020

Abstract

Structural and electrical features of p-type neodymium-doped GaSe single crystal (0.1 at.% Nd) grown by modified Bridgman technique was investigated through X-ray diffraction (XRD) and current–voltage (*I–V*) measurements. The XRD spectrum reveals that GaSe:Nd single crystal investigated has hexagonal structure ($a = 3.750$ Å, $c = 15.950$ Å and $z = 4$, P63/mmc space group) with preferred orientation along (004). Ohmic contact was realized by evaporating indium (In) on one surface of the GaSe:Nd single crystal at 10^{-6} Torr while Shottky contact was obtained by evaporating twelve Au dot contacts with 7.85×10^{-3} cm^2 area on the other surface of the crystal. The *I–V* characteristics of Au/GaSe:Nd/In Schottky contact was analysed in the 100–360 K temperature range. The main Schottky diode parameters such as ideality factor, barrier height and the series resistance values were determined as a function of temperature using conventional *I–V* method and Norde method. The ideality factor *n* of the Au/GaSe:Nd/In Schottky contact was observed to decrease while the barrier height Φ_b increased with increasing temperature. Temperature dependence of the diode parameters were attributed to the existence of barrier height inhomogeneity by assuming a Gaussian distribution of Au/GaSe:Nd/In Schottky contact.

1 Introduction

As a layered single crystal, GaSe is formed by the stacking of Se–Ga–Ga–Se atoms in two-dimensional layers with four polytpes depending on the stacking of the layers [1–4]. The difference between interatomic (covalent) and interlayer (van der Waals) bonding causes a strong anisotropy in these crystals. Weak interlayer interactions makes easy cleavage possible along the *c*-axis [3–7].

GaSe single crystal has direct and indirect band gap energies of about 2.02 eV and 2.1 eV at room temperature [3, 4, 8] which make it a potential material for LEDs, Schottky barrier diodes (SBDs), radiation detectors, photoconductor, spintronic, photoelectronic and optoelectronic devices and non-linear optical applications [1–10]. The transmission range of GaSe single crystal extends from 0.65 to 18 μm [7–9, 11, 12]. GaSe crystals have been doped with different atoms to control and modify the structural, optical and electrical properties [1, 5–7, 9, 12–18]. These crystals can exhibit both *p*- and *n*-type conductivity depending on the experimental conditions and composition. For instance, Cl and Ge-doped GaSe crystals show n-type conductivity [14, 17] while Gd, As and Sb doped crystals show p-type conductivity [13, 14, 16]. The structural properties of undoped and doped GaSe crystals have been studied by XRD and Raman spectroscopy [2–4, 6, 19, 20] while the electrical properties of GaSe have been studied by current–voltage (*I–V*) and Hall effect measurements [21–24]. Resistivity and Hall mobility measurements conducted in the 77–850 K temperature interval revealed five acceptor levels in the 31–310 meV range [22]. Activation energies of GaSe crystals annealed at 500 °C and 700 °C were found to be between 234–267 and 26–74 meV at 100–190 K and 200–320 K temperature ranges, respectively [23]. Tin was shown to behave as a double-acceptor level in GaSe with ionization energies of 155 and 310 meV [24]. Three trap levels were determined at 0.02 eV, 0.10 eV and 0.26 eV from the thermally stimulated current measurements of layered GaSe single crystals conducted in the 10–300 K temperature interval [21]. Several

✉ Hüseyin Ertap
huseyinertap@gmail.com; huseyinertap@kafkas.edu.tr

✉ Sakir Aydogan
saydogan@atauni.edu.tr

[1] Department of Physics, Faculty of Science and Letters, Kafkas University, 36100 Kars, Turkey

[2] Department of Physics, Faculty of Sciences, Atatürk University, 25240 Erzurum, Turkey

[3] Department of Electrical and Electronics Engineering, Ardahan University, 75000 Ardahan, Turkey

[4] Department of Physics, Gebze Technical University, 41400 Gebze/Kocaeli, Turkey

parameters of SBDs have also been identified for undoped and Gd-doped GaSe crystals [13, 25–27].

In the present study, we have investigated the structural and electrical properties of Nd-doped GaSe crystal through XRD and temperature-dependent *I–V* measurements. To the best of our knowledge, there is no experimental data available on the current-transport mechanism and Schottky diode application of Nd-doped GaSe crystals in the literature. Hence, the data presented will make important contribution in understanding the device application potentials of Nd-doped GaSe crystals.

2 Experimental

The p-type neodymium-doped GaSe single crystal (0.1 at.% Nd) was grown by modified Bridgman technique using high purity Ga (99.9999%), Se (99.9999%) and Nd (99.999%) in evacuated quartz ampoules. The crystal growth details were described in our previous study [1]. The ingot obtained was bright red in color with mirror-like surfaces, characteristic of layered structures. For the measurements, ingots were cleaved using razor blade into about 10 mm × 10 mm platelets with an average thickness of 170 µm. The XRD pattern of the 0.1 at.% Nd-doped GaSe single crystal was recorded on a Bruker D8 Discovery diffractometer with Cu-K_α radiation ($\lambda = 1.5418$ Å).

The ohmic contact was made on the perfect mirror surface of GaSe:Nd single crystal by thermal evaporation of In at 10^{-6} Torr and it was annealed at 300 °C for 5 min. in N_2 atmosphere. Then, twelve Au dot circle contacts with 7.85×10^{-3} cm^2 area were evaporated on the other perfect mirror surface of GaSe:Nd at 10^{-6} Torr for Schottky contacts. Thus, one Au/GaSe:Nd/In Schottky contact having the best performance was selected and analysed in detail through *I–V* measurements in the 100–360 K temperature range. The *I–V* measurements of the Au/GaSe:Nd/In Schottky contact were conducted with a Keithley 487 Picoammeter/Voltage Source in dark.

3 Results and discussion

The XRD spectrum of GaSe:Nd single crystal is given in Fig. 1 which is similar to the pattern observed our previous study of undoped and Dy doped GaSe single crystals [8]. Analysis of XRD spectrum shows that the GaSe:Nd single crystal grew in hexagonal structure with lattice parameters $a = 3.750$ Å, $c = 15.950$ Å and $z = 4$ belonging to the P63/mmc space group (JCPDS-Card No: 37-0931), the same as the undoped GaSe single crystal. The strongest diffraction peak of GaSe:Nd was observed around $2\theta = 22.632°$ in the XRD pattern corresponding to diffraction from the (004) plane.

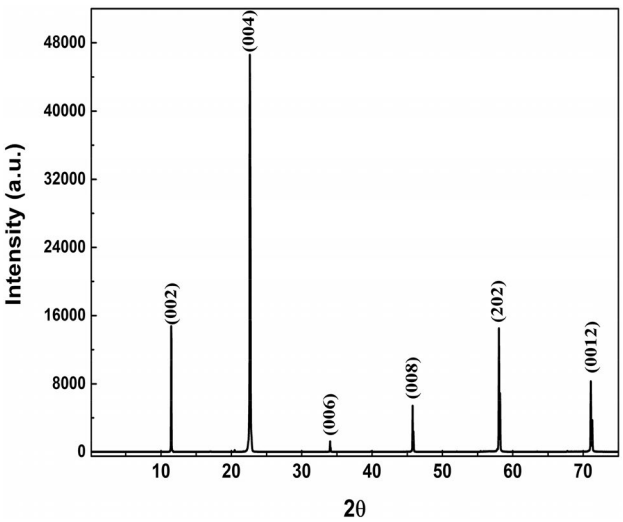

Fig. 1 The XRD spectrum of GaSe:Nd single crystal

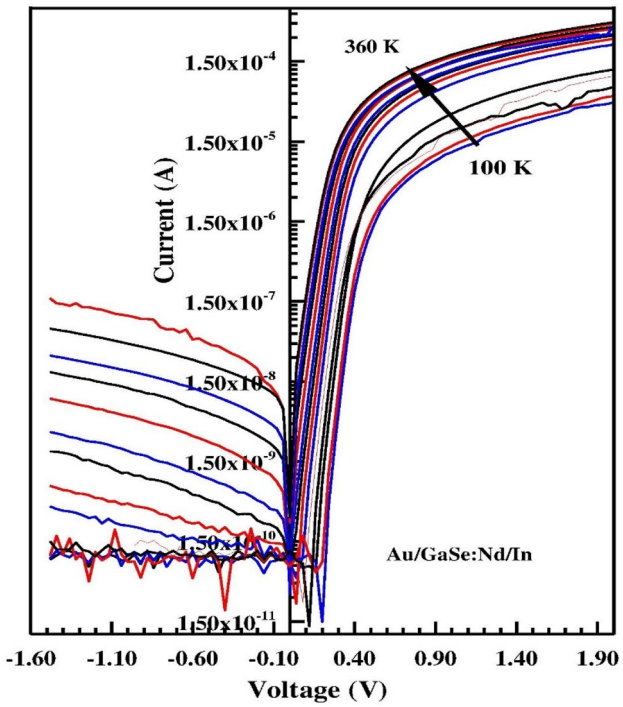

Fig. 2 The current–voltage plots of Au/GaSe:Nd/In Schottky diode as a function of temperature

Figure 2 shows the current–voltage plots of Au/GaSe:Nd/In Schottky diode as a function of temperature. The measurements have been carried out between 100 and 360 K with 20 K steps. It is clearly seen that the *I–V* characteristics of Au/GaSe:Nd/In Schottky diodes show two regions of forward current transport which are affected by

temperature. The low-voltage linear region is governed by thermionic emission (TE), namely the forward bias *I–V* curves are linear on the semi-logarithmic scale from 0.0 to 0.4 V and start deviating from linear behavior afterwards. In the high voltage bias region, it is assumed that mechanisms like the recombination current in the space charge region [28] or the series resistance effect leads to the deviation from the straight line [29]. Since the current flow is caused by the carriers jumping over a barrier in the Schottky diodes, more electrons will pass through the barrier as the temperature increases, so the current will increase with increasing temperature as seen in Fig. 2. Hence, the TE theory [30] was used in the evaluation of the *I–V* characteristics for lower biases. According to the TE, the relation between current (*I*) and voltage (*V*) for a Schottky diode is given by:

$$I = I_0\left[\exp\left(\frac{qV}{nkT}\right) - 1\right], \tag{1}$$

where I_o is the reverse saturation current expressed by:

$$I_o = AA^*T^2 \exp\left(-\frac{q\Phi_b}{kT}\right), \tag{2}$$

The saturation current I_o is determined using the intercept on the current axis of the ln*I* at zero-bias. In Eq. 2, *q* is the electron charge, *k* is the Boltzmann's constant, *T* is the temperature in Kelvin, *A** is the Richardson constant and its value is 247 A/cm^2 K^2 for GaSe [31], and *A* is the effective diode area ($A = 7.85 \times 10^{-3}$ cm^2). Φ_b is the Schottky barrier height at zero bias which is determined from Eq. 2. The ideality factor *n* is a measure of conformity of the junction to pure TE which is determined by the slope of the ln*I–V* plot through the relation:

$$n = \frac{q}{kT}\frac{dV}{d(\ln I)}. \tag{3}$$

The value of *n* is unity (1) for perfect rectifying junctions. However, it may not be possible to achieve a value of 1 in practice due to the bias voltage dependence of the barrier height, presence of the interfacial thin layer between metal and semiconductor, the higher series resistance of the Schottky diode especially appearing at higher bias, the barrier inhomogeneities and so on. *n* values greater than 1 degrades the device performance.

Twelve Au/GaSe:Nd/In Schottky diodes were prepared under identical conditions. A plot of experimental barrier height against the ideality factor of the Au/GaSe:Nd/In Schottky diodes at the same temperature will give information about the homogeneity of the diode. We have performed the *I–V* measurements of all diodes at 300 K and then calculated the experimental ideality factors and the barrier heights of twelve diodes. The ideality factors of the diodes ranged from 1.21 to 1.88 and the barrier heights from 0.51 to 0.83 eV, respectively. We have observed higher ideality factors for lower barrier heights which is explained by the nonuniform interfaces and by lateral inhomogeneities of the barrier height [32, 33].

The homogeneous barrier height has been calculated to be 0.64 eV. Furthermore, the average effective Schottky barrier height of 0.68 ± 0.11 eV and the average ideality factor of 1.42 ± 0.14 were determined from the experimental *I–V* plots for the Au/GaSe:Nd/In Schottky contacts. The diode having the lowest ideality factor and highest barrier height has been studied in detail as described below. Kurtin and Mead have studied the barrier height of metal contacts on GaS, GaSe, GaTe layered semiconductors, using the photoresponse technique and analysed the dependence of barrier height on the electronegativity of contact metals. They have found a lower barrier height value of 0.45 eV for Au/p-GaSe Schottky diode which is lower than the barrier height of 0.83 eV we obtained for the Au/p-GaSe Schottky diode at room temperature. This discrepancy in Φ_b values may result from the differences in the fabrication techniques or experimental preparation of the devices. It is desirable, however, to obtain rectifier contacts with a higher barrier height, since the high barrier height of rectifier contacts increase the rectification rate of the device [34, 35].

n–T and Φ_b–*T* plots of Au/GaSe:Nd/In Schottky diode are given in Fig. 3. As seen, the measured ideality factors decreased with increasing temperature. This decrease is very sharp between 100 and 200 K and moderate between 200

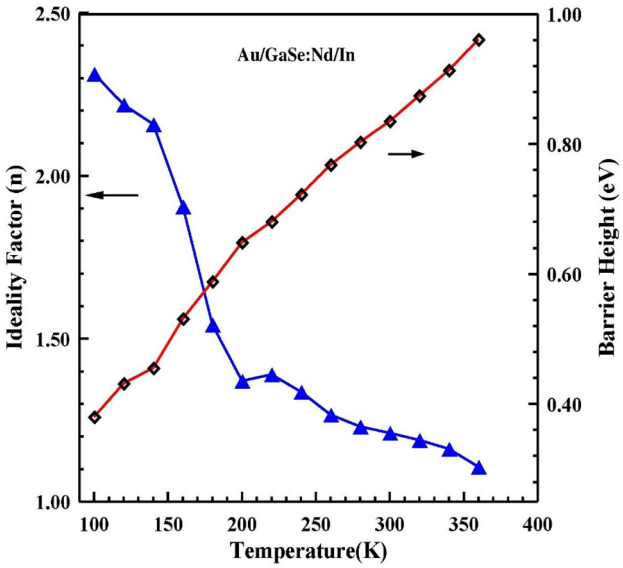

Fig. 3 *n–T* and Φ_b–*T* plots of Au/GaSe:Nd/In Schottky diode for various temperatures

and 360 K. The experimental values of n range from 2.31 (at 100 K) to 1.11 (at 360 K). The n value greater than 1 could be attributed to other mechanisms aside the TE such as the image force effect, recombination-generation processes or tunneling. A wide distribution of low-barrier height patches may be the reason for the high n value [36]. The barrier heights were determined from TE [30] using:

$$\Phi_b = \frac{kT}{q}\ln\left(\frac{AA^*T^2}{I_0}\right). \quad (4)$$

The experimental Φ_b values for Au/GaSe:Nd/In Schottky diode were found to be in the 0.38 eV (at 100 K) and 0.96 eV (at 360 K) range. The variation of barrier heights with temperature is also plotted in Fig. 3. It is seen that the barrier heights increase with increasing temperature while the ideality factor shows the opposite behavior, i.e., it decreases. Furthermore, this variation of the ideality factor and the barrier height with temperature is clear evidence of the deviation from TE theory in its current conduction mechanism. For example, current transport of Au/GaSe:Nd/In Schottky diode may be occurring through lower patches [37]. Figure 4 depicts the plot of experimental ideality factor versus the barrier height for the Au/GaSe:Nd/In Schottky diode as a function of temperature. Two linear regions are observed between the experimental zero-bias barrier heights and ideality factors of the Au/GaSe:Nd/In Schottky diode. The linear relation between barrier height and ideality factor confirms the lateral inhomogeneities of the barrier height and shows a discontinuity at the Au/GaSe:Nd/In interface [33, 38–41]. Furthermore, this curve allows one to determine the barrier heights for an ideal junction diode. This behavior indicates two activated processes with different average barrier heights which were fit separately. For an ideal Schottky diode, the extrapolation of ϕ_b and n gives the mean values for ϕ_b which were determined to be 1.12 eV for region I and 0.74 eV for region II, respectively, in the present study. The laterally homogeneous barrier height has been calculated as 0.64 eV from extrapolation to $n=1$ for the Au/GaSe:Nd/In Schottky contacts using the linear relationship between the effective barrier heights and the ideality factors. It is known that the device preparation environment, measurement system and the temperature dependence of the band gap may also contribute to the fluctuations in barrier heights with temperature.

The Richardson plot may be drawn to obtain the barrier height of the Schottky diode analysed in a wide temperature range in addition to conventional TE theory [42]. The Richardson plot of the Au/GaSe:Nd/In Schottky diode for various temperatures has been obtained by rewriting Eq. 2 as:

$$\ln\left(\frac{I_0}{T^2}\right) = \ln(AA^*) - \frac{q\overline{\Phi}_{b0}}{kT}. \quad (5)$$

Richardson plot obtained using Eq. 5 is given in Fig. 5. The mean barrier height $\overline{\Phi}_{bo}$ and Richardson constant A^* are determined from the slope and intercept of this straight line. The Φ_{b0} value and A^* are determined as 0.16 eV and 6.5×10^{-10} A/cm^2 K^2, respectively. The deviation in the value of the Richardson constant from theoretical value may result from the presence of the spatially inhomogeneous barrier

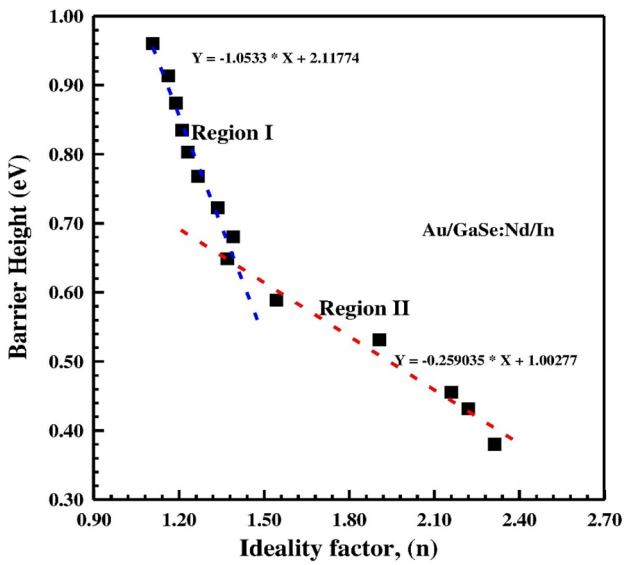

Fig. 4 The plot of experimental barrier height versus the ideality factor for the Au/GaSe:Nd/In Schottky diode for various temperatures

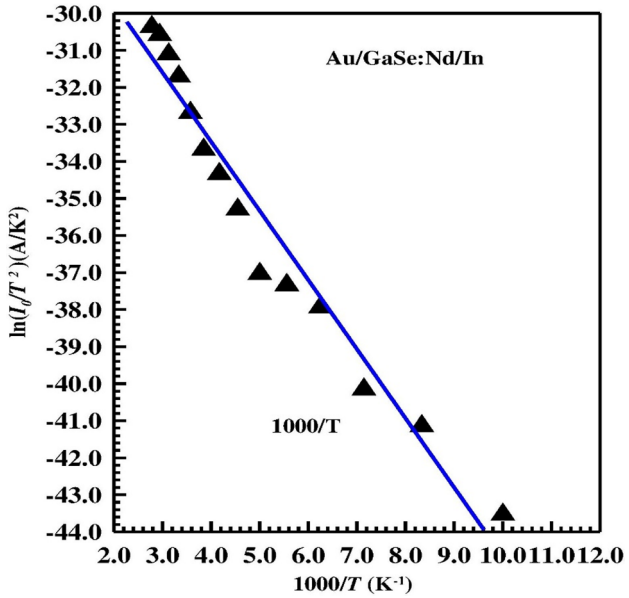

Fig. 5 The Richardson plot of Au/GaSe:Nd/In Schottky diodes obtained over a temperature range of 100–360 K

height in addition to the potential fluctuations at the interface of the Au/GaSe:Nd/In Schottky diode. The current mechanism of Schottky diode depends on temperature, which means that when the temperature is increased, the current flows preferentially through the higher barrier areas. The voltage dependence of the barrier height can be determined from the barrier inhomogeneity model using the temperature dependence of ideality factor n, as below [36, 43, 44]:

$$-\frac{\partial \Phi_b}{\partial V} = \left(\frac{1}{n} - 1\right) = -\rho_2 + \frac{q\rho_3}{2kT}. \tag{6}$$

In Eq. 6, ρ_2 and ρ_3 are the voltage coefficients, the former being dimensionless, which may depend on T. The coefficients ρ_2 and ρ_3 quantify the voltage deformation of the Φ_b distribution [39]. Figure 6 depicts $[(1/n) - 1]$ vs $1/2kT$ plot of the Au/GaSe:Nd/In Schottky diodes. The linearity of the curve implies that the ideality factor expresses the voltage deformation of the Gaussian distribution of the SBDs. The coefficients ρ_2 and ρ_3 are determined to be $\rho_2 = 0.0833$, $\rho_3 = 0.0266$ V from the intercepts and gradient, respectively, from Fig. 6.

Norde method [45] is used to determine the values of the series resistance and barrier height via forward bias I–V measurements. For this purpose, the function $F(V)$ is described as:

$$F(V) = \frac{V}{\beta} - \frac{kT}{q} \ln\left(\frac{I(V)}{AA^*T^2}\right), \tag{7}$$

where β is the first integer (dimensionless) greater than ideality factor n. In the evaluation of Eq. 7, first, the F vs. V curve is obtained and then the minimum of the F vs. V is deterimined. After that, the value of barrier height can be determined from Eq. (8):

$$\Phi_b = F(V_0) + \frac{V_0}{\beta} - \frac{kT}{q}, \tag{8}$$

where $F(V_0)$ and V_0 are the minimum point of $F(V)$ and V, respectively. Figure 7 shows the $F(V)$–V plots of the Au/GaSe:Nd/In Schottky diodes as a function of temperature. Furthermore, the series resistance R_s of a Schottky diode is determined using Norde's functions via Eq. 9:

$$R_s = \frac{kT(\beta - n)}{qI}. \tag{9}$$

Figure 8 shows the barrier height and the series resistance determined from the Norde method of the Au/GaSe:Nd/In Schottky diodes as a function of temperature. The temperature-dependent series resistance and barrier height values are calculated and these are given in Table 1. As seen, both parameters vary with temperature: the R_s decreased while Φ increased with temperature. The variation of the barrier heights with temperature has been explained above. In addition, Norde's method can be used to obtain the experimental barrier height when TE is the dominant conduction mechanism [46]. Both methods use

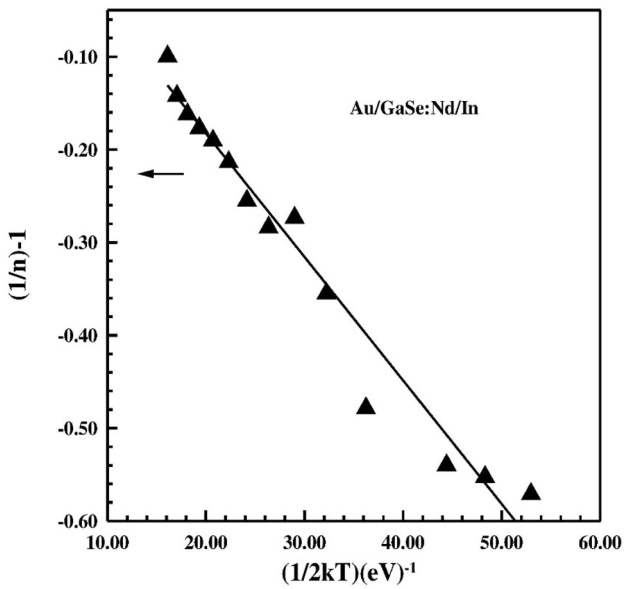

Fig. 6 The $[(1/n) - 1]$ vs $1/2kT$ plot of Au/GaSe:Nd/In Schottky diodes

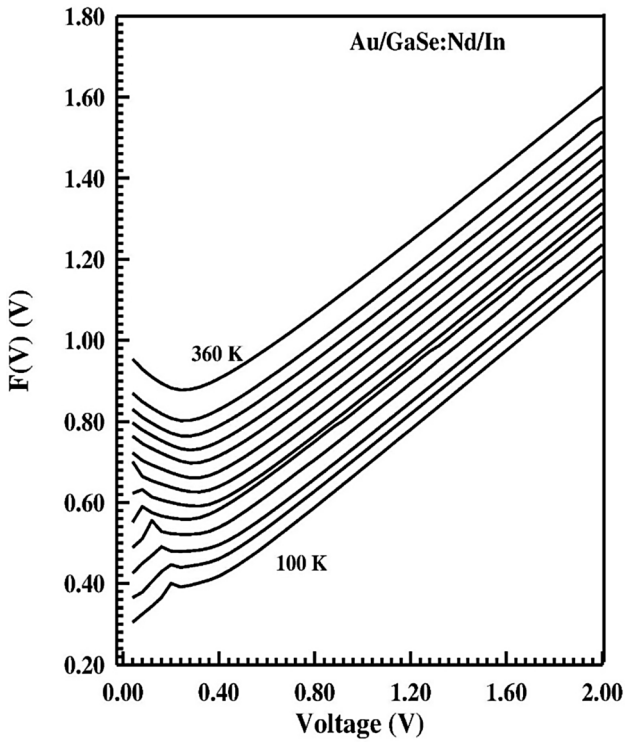

Fig. 7 The $F(V)$–V plots of the Au/GaSe:Nd/In Schottky diodes as a function of temperature

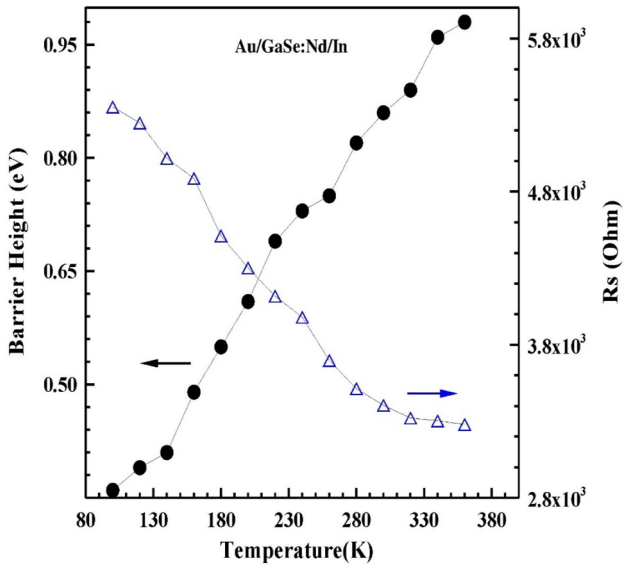

Fig. 8 The barrier height and the series resistance of the Au/GaSe:Nd/In Schottky diodes as a function of temperature determined from the Norde method

Table 1 Temperature-dependent electrical parameters of Au/GaSe:Nd/In Schottky diodes determined from *I–V–T* measurements

Temperature (K)	*I–V*		Norde	
	n	Φ_b (eV)	Φ_b (eV)	R_s (Ω)
100	2.31	0.38	0.36	5354
120	2.22	0.43	0.39	5249
140	2.16	0.45	0.41	5019
160	1.90	0.53	0.49	4887
180	1.54	0.59	0.55	4512
200	1.37	0.65	0.61	4302
220	1.39	0.68	0.69	4118
240	1.34	0.72	0.73	3980
260	1.26	0.77	0.75	3698
280	1.23	0.80	0.82	3514
300	1.21	0.83	0.86	3405
320	1.19	0.87	0.89	3322
340	1.16	0.91	0.96	3304
360	1.11	0.96	0.98	3280

the forward bias region of *I–V* plots and both calculate the effective barrier height value as a function of temperature as seen in Eqs. 4 and 7. Thus, the barrier height values obtained from both techniques are expected to be compatible with each other owing to the use of TE mechanism. The decrease of the series resistance values with the increasing temperature is attributed to the increase of the free carrier concentration due to de-trapping of the carriers at the interface of Au/GaSe:Nd/In Schottky diodes [47].

4 Conclusion

We have presented the structural and electrical properties of Nd-doped GaSe single crystal, grown by Bridgman method. The XRD analysis showed that Nd-doped GaSe single crystal grew with the same hexagonal structure as the undoped GaSe single crystal. The electrical properties of Au/GaSe:Nd/In Schottky diodes was investigated through the current–voltage (*I–V*) measurements in the 100–360 K temperature range. The ideality factor, the barrier height and the series resistance have been determined and it was seen that all parameters depend on temperature. The ideality factor *n* ranged from 2.31 (at 100 K) to 1.11 (at 360 K) while the barrier height Φ_b ranged from 0.38 eV (at 100 K) to 0.96 eV (at 360 K) from conventional *I–V* plots. These variation of *n* and Φ_b has been attributed to the barrier inhomogeneities by assuming a Gaussian distribution of Au/GaSe:Nd/In Schottky diode interface. Similar variation of Φ_b was obtained using Norde method. Series resistance decreased with increasing temperature. This opposite variation of *n* and Φ_b with temperature has been explained in terms of barrier height inhomogeneities at the interface of Au and GaSe:Nd.

References

1. A. Karatay, M. Yuksek, H. Ertap, A. K. Mak, M. Karabulut, A. Elmali, Opt. Mater. **64**, 74–80 (2016)
2. H. Karaağaç, M. Parlak, O. Karabulut, U. Serincan, R. Turan, B.G. Akınoğlu, Cryst. Res. Technol. **41**, 1159–1166 (2006)
3. A. Gouskov, J. Camassel, L. Gouskov, Prog. Cryst. Growth Charact. **5**, 323–413 (1982)
4. N.C. Fernelius, Prog. Cryst. Growth Charact. Mater. **28**, 275–353 (1994)
5. V. Capozzi, Phys. Rev. B **28**, 4620–4627 (1982)
6. K. Allakhverdiev, T. Baykara, Ş. Ellialtioğlu, F. Hashimzade, D. Huseinova, K. Kawamura, A.A. Kaya, A.M. Kulibekov, S. Onari, Mater. Res. Bull. **41**, 751–763 (2006)
7. C. Kim, K. Jang, Y. Lee, Solid State Commun. **130**, 701–704 (2004)
8. H. Ertap, M. Yuksek, A. Karatay, A. Elmali, M. Karabulut, Chin. J. Phys. **59**, 465–472 (2019)
9. H. Ertap, Opt. Mater. **83**, 99–103 (2018)
10. O. Karabulut, M. Parlak, R. Turan, U. Serincan, B.G. Akınoğlu, Cryst. Res. Technol. **41**, 243–249 (2006)
11. N.B. Singh, R. Narayanan, A.X. Zhao, V. Balakrishna, R.H. Hopkins, D.R. Suhre, N.C. Fernelius, F.K. Hopkins, D.E. Zelmon, Mater. Sci. Eng. B **49**, 243–246 (1997)
12. A. Karatay, M. Yuksek, H. Ertap, A. Elmali, M. Karabulut, Opt. Laser Technol. **99**, 392–395 (2018)
13. S. Duman, B. Gürbulak, S. Doğan, T.B. Tekle, Phys. E **42**, 1958–1962 (2010)
14. S. Shigetomi, T. Ikari, H. Nakashima, Jpn. J. Appl. Phys. **39**, 5083–5084 (2000)
15. G. Micocci, A. Serra, A. Tepore, Phys. Status Solidi (a) **162**, 649–659 (1997)
16. S. Shigetomi, T. Ikari, H. Nishimura, Jpn.J. Appl. Phys. **32**, 2731–2734 (1993)

17. G. Micocci, A. Serra, A. Tepore, J. Appl. Phys. **82**, 2365–2369 (1997)
18. M. Yuksek, A. Karatay, H. Ertap, A. Elmali, M. Karabulut, Opt. Mater. **66**, 137–141 (2017)
19. A. Kuhn, A. Chevy, R. Chevalier, Phys. Status Solidi (a) **31**, 469–475 (1975)
20. J.C.J.M. Terhell, W.C. van der Vleulen, Mater. Res. Bull. **11**, 101–106 (1976)
21. N.M. Gasanly, A. Aydınlı, Ö. Salihoğlu, Cryst. Res. Technol. **36**(3), 295–301 (2001)
22. C. Manfredotti, A. M. Mancini, R. Murri, A. Rizzo, L. Vasenelli, II Nuovo Cimento **39**(1), 257–268 (1977)
23. O. Karabulut, M. Parlak, R. Turan, U. Serincan, E. Tasarkuyu, B.G. Akinoglu, Cryst. Res. Technol. **38**, 811–816 (2003)
24. J.F. Sanchez-Royo, D. Errandonea, A. Segura, J. Appl. Phys. **83**(9), 4750–4755 (1998)
25. S. Duman, B. Gürbulak, S. Doğan, A. Türüt, Vacuum **85**, 798–801 (2011)
26. W.C. Huang, C.T. Horng, Y.M. Chen, Y.K. Hsu, C.S. Chang, Phys. Status Solidi (c) **10**, 3405–3409 (2008)
27. W.C. Huang, S.H. Su, Y.K. Hsu, C.C. Wang, C.S. Chang, Superlattices Microstruct. **40**, 644–650 (2006)
28. B. Akkal, Z. Benamara, A. Boudissa, N. Bachirbouidjra, M. Amrani, L. Bideux, B. Gruzza, Mater. Sci. Eng. B **55**, 162–168 (1998)
29. Y. Kribes, I. Harrisson, B. Tuck, T.S. Cheng, C.T. Foxon, Semicond. Sci. Technol. **12**, 913–916 (1997)
30. E.H. Rhoderick, R.H. Williams, *Metal Semiconductor Contacts* (Clarendon Press, Oxford, 1988)
31. K. Çınar Demir, Ş. Aydoğan, E. Gür, C. Coşkun, Z. Aygün, Radiat. Effects Defects Solids **172**, 650–663 (2017).
32. Ş. Aydoğan, K. Çınar, H. Asıl, C. Coşkun, A. Türüt, J. Alloys Compd. **476**, 913–918 (2009)
33. R.F. Schmitsdorf, T.U. Kampen, W. Mönch, J. Vacuum Sci. Technol. B **15**, 1221–1226 (1997)
34. S. Kurtin, C.A. Mead, J. Phys. Chem. Solids **29**, 1865–1867 (1968)
35. S. Kurtin, C.A. Mead, J. Phys. Chem. Solids **30**, 2007–2009 (1969)
36. R.T. Tung, Phys. Rev. B **45**, 13509–13523 (1992)
37. Ş. Aydoğan, M. Sağlam, A. Türüt, Appl. Surf. Sci. **250**, 43–49 (2005)
38. S. Chand, J. Kumar, Semicond. Sci. Technol. **11**, 1203–1208 (1996)
39. Ş. Karataş, Ş. Altındal, A. Türüt, A. Özmen, Appl. Surf. Sci. **217**, 250–260 (2003)
40. R.F. Schmitsdorf, T.U. Kampen, W. Mönch, Surf. Sci. **324**, 249–256 (1995)
41. V.R. Reddy, V. Janardhanam, C.H. Leem, C.J. Choi, Superlattices Microstruct. **67**, 242–255 (2014)
42. Z. Khurelbaatar, K.H. Shim, J. Cho, H. Hong, V.R. Reddy, C.J. Choi, Mater. Trans. **56**, 10–16 (2015)
43. A. Ahaitouf, H. Srour, S.O.S. Hamady, N. Fressengeas, A. Ougazzaden, J.P. Salvestrini, Thin Solid Films **522**, 345–351 (2012)
44. J.H. Werner, H.H. Güttler, J. Appl. Phys. **69**, 1522–1533 (1991)
45. H. Norde, J. Appl. Phys. **50**, 5052–5053 (1979)
46. A. Türüt, Turk. J. Phys. **36**, 235–244 (2012)
47. Ş. Aydoğan, M. Sağlam, A. Türüt, Y. Onganer, Mater. Sci. Eng. C **29**, 1486–1490 (2009)